

An Extreme Learning Machine Approach to Predicting Near Chaotic HCCI Combustion Phasing in Real-Time

Adam Vaughan

Dept. of Mechanical Engineering
University of Michigan
Ann Arbor, MI USA
vaughana@umich.edu

Stanislav V. Bohac

Dept. of Mechanical Engineering
University of Michigan
Ann Arbor, MI USA
sbohac@umich.edu

October 14th, 2013*

Abstract

Fuel efficient Homogeneous Charge Compression Ignition (HCCI) engine combustion phasing predictions must contend with non-linear chemistry, non-linear physics, period doubling bifurcation(s), turbulent mixing, combustion deposits, model parameters that can drift day-to-day, and air-fuel mixture state information that cannot typically be resolved on a cycle-to-cycle basis, especially during transients. In previous work, a generalized cycle-to-cycle mapping function coupled with ϵ -Support Vector Regression was shown to predict experimentally observed cycle-to-cycle phasing over a wide range of engine conditions, despite some of the aforementioned difficulties. The main limitation of the previous approach was that a partially acausal randomly sampled training dataset was used to train proof of concept offline predictions. The objective of this paper is to address this limitation by proposing a new online adaptive Extreme Learning Machine (ELM) extension named Weighted Ring-ELM. This extension enables fully causal phasing predictions at randomly chosen engine set points, and is shown to achieve results that are as good as or better than the previous offline method. The broader objective of this approach is to enable a new class of real-time model predictive control strategies for high variability HCCI and, ultimately, to bring HCCI's low engine-out NO_x and high fuel efficiency to production engines.

Introduction

HCCI is an advanced engine combustion technique that uses unthrottled low temperature autoignition of lean air-fuel mixtures to achieve high fuel efficiency and low engine-out NO_x (a smog precursor) compared to traditional combustion techniques such as spark ignition or Diesel combustion. While the use of autoignition is the central idea behind HCCI, autoignition itself is difficult to predict and there is no direct actuator to control its timing relative to the motion of the piston (e.g. a spark).

A key challenge for gasoline engine HCCI is generating a high enough air-fuel mixture temperature to ensure autoignition [1]. This is commonly achieved by carrying over

a sizable fraction (typically 20-60% [2, 3]) of residual gases from the previous burn to promote combustion on the next cycle using Negative Valve Overlap (NVO). While convenient for a number of practical reasons described in [1], the use of residual gases introduces strong cycle-to-cycle coupling on top of the already non-linear chemistry and physics that occur throughout a complete engine cycle [4]. Further compounding the issues with residual gases is that neither the airflow to the cylinder(s) nor the quantity of residual gases in the cylinder can be accurately resolved before a burn happens on a *cycle-to-cycle* (not mean value) basis with commonly available sensors, especially during transients. Beyond residual gas influences, there are also complex secondary influences on combustion behavior such as turbulent mixing, manifold resonance effects, combustion deposits, different varieties of fuel and even ambient temperature variations [5, 6].

While HCCI is already a significant challenge given the above complexity, the combustion mode also exhibits a period doubling bifurcation cascade to chaos [4, 7, 8], similar to what is seen in high residual spark ignition engines [9]. When nearly chaotic, HCCI is still deterministic but becomes oscillatory and very sensitive to parameter variations (e.g. residual gas fraction fluctuations [7, 8]). This oscillatory "stability limit" behavior is commonly referred to as high Cyclic Variability (CV) and it severely constrains the available load limits of HCCI.

Motivation and goals

A primary constraint for HCCI is the need to keep combustion phasing between the ringing and combustion stability limits [10]. At the ringing limit, excessive pressure rise rates are encountered, and at the stability limit, high CV in combustion phasing is observed [10]. Since these limits play a key role in constraining HCCI's usable operating range, it is desirable to explore new methods to predict the behavior at and beyond these constraints. In particular, the ability to predict and correct for high CV might enable the use of late phased combustion to mitigate the excessive pressure rise rates that currently constrain HCCI's high-load operation [11], while also potentially addressing the high CV experienced at low-load. Towards the end goal of expanding the HCCI load envelope, this paper builds on previous work [4] by describing a new online adaptive learning

*There are no fundamental changes in this updated version of the original October 14th, 2013 paper. This version includes algebraic simplifications, minor corrections, and improved body text.

method that enables fully causal cycle-to-cycle phasing predictions across randomly chosen engine set point transients that include both stable and the near chaotic bifurcation behavior described in [4, 7, 8].

Experimental Observations

In the authors’ previous publication [4], engine combustion was abstracted into a generalized mapping function within the framework of a discrete dynamical system:

$$\begin{aligned} \text{next combustion} = \\ \text{function}(\text{previous combustion}, \text{parameters}) \end{aligned} \quad (1)$$

This abstraction was intended to convey a conceptual understanding of the experimental cycle-to-cycle behavior seen in Fig. 1’s return maps.

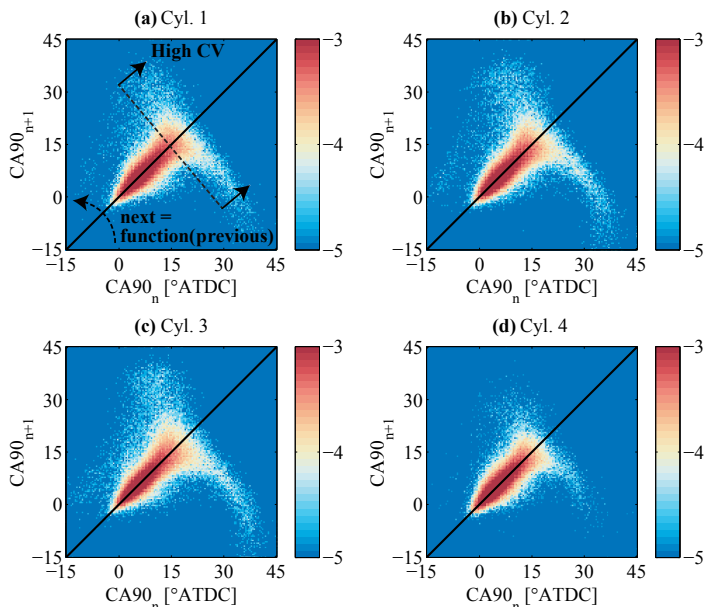


Figure 1: Return map probability histograms of CA90 generated from 129,964 cycles and 2,221 random engine set points. Outliers are omitted and total only $\sim 3\%$ of the data. The colormap is \log_{10} to show order of magnitude differences. [4]

These return maps show the experimentally observed combustion timing for a given cycle n along the abscissa and the next cycle $n + 1$ along the ordinate under random engine actuator set points [4]. The value CA90 is the time in Crank Angle Degrees ($^{\circ}\text{CA}$) where 90% of the fuel’s net heat release is achieved, and thus measures the timing of the end of the burn in relation to piston’s position as the crank rotates. The reader should note that there is structure to the cycle-to-cycle behavior despite the random actuator set points used to generate Fig. 1.* The structure shows a deterministic transition to oscillatory high CV behavior as combustion moves towards later phasing, which can be viewed as at least a single period doubling bifurcation with sensitive dependence

*While it is not shown here, there is similar structure in CA10 and CA50 percent burn metrics, although less pronounced (especially in CA10) [4]. Since CA90 is a stronger indicator of the oscillatory behavior seen at later combustion phasing, it is used as the main combustion input to the model that will be described in later sections.

on the engine set point [4, 7, 8]. While mathematically interesting, this oscillatory high CV structure undesirably constrains practical HCCI engine operation. A more thorough description of these data is provided in [4].

Modeling Approaches

In [4], a skeletal functional form for the general mapping function was built out using measurable quantities, thermodynamics and known correlations. Then, unlike the physics-based approaches that are usually discussed in the engine literature, the machine learning technique of ϵ -Support Vector Regression (ϵ -SVR) was combined with the skeletal functional form to provide quantitative predictions. The primary motivation for this machine learning approach was not that existing chemical kinetics with Computational Fluid Dynamics (CFD) cannot capture engine behavior (see [12] and gasoline mechanism validation [13]) but that the methods are:

- Too computationally intensive for real-time predictions.
- Subject to experimental uncertainties in the *cycle-to-cycle* (not mean value) mixture state and composition.

As a point of reference, the simulation time of a 2,500 RPM, 48 millisecond engine cycle is measured in $\sim \text{day(s)}$ for a single core of a modern computer.

At the other computational complexity extreme, low-order approximation models of HCCI for control have been developed since at least the early 2000’s [14], based on spark ignition engine knock models developed in the 1950’s [15]. Recently, efforts have been made to extend this type of model to the high CV regions of HCCI by injecting random residual fraction noise to capture uncertainties in mixture state and composition [8]. This model was tuned for a limited set of steady-state conditions and only “predictive” in the sense that when injected with random (i.e. unpredictable) noise could it capture the general return map shape seen experimentally. That said, the model is useful for theoretically showing that a period doubling cascade to chaos driven by residual gas fraction underlies the observed high CV behavior.

In the context of the above, machine learning provides a computationally efficient way to capture complex combustion patterns while simultaneously avoiding explicit knowledge of the underlying mixture state and composition (provided an appropriate abstract mapping function is chosen). While there are clearly benefits to this machine learning approach, a key issue is that machine learning is data driven, and relatively large quantities of data are needed to adequately cover large dimensional spaces. As shown conceptually in Fig. 2, these high dimensional data might be viewed as a “porcupine” [16]. Each engine operating condition might be viewed as a “quill” of Eq. 2’s six-dimensional “porcupine,” and machine learning algorithms know nothing about the ideal gas law or chemical kinetics, so their ability to extrapolate between “quills” is limited, especially when provided sparse data. Previous work [4] used a random sampling of cycle time series for training to ensure the data driven model had data to fit the “quills,” and then assessed the model’s ability to predict on the remaining (ran-

domly chosen) cycles. Thus, the training dataset was partially acausal and that the model itself wasn't shown to adapt to new conditions.

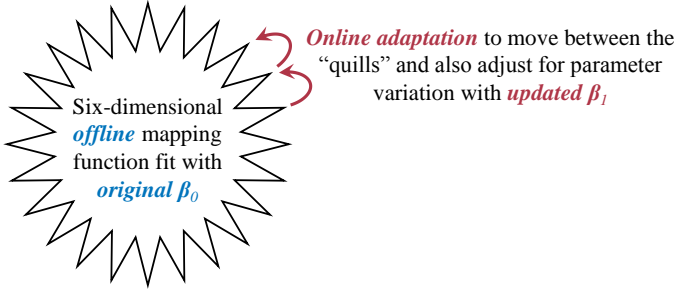


Figure 2: High dimensional data might be viewed conceptually as a “porcupine” [16]. The primary goal of this paper is to design an online adaptive algorithm to fit new data between the “quills.”

Contribution

The primary contribution of this work is the development of a new online learning method to provide real-time adaptive, fully causal predictions of HCCI combustion phasing. This method, called Weighted Ring - Extreme Learning Machine (WR-ELM), enables online extrapolation of an offline Extreme Learning Machine (ELM) model that is trained to fit the “quills” of offline data.

Methods

Mapping Function Modifications

In previous work [4], engine combustion was abstracted to the following generalized mapping function:

$$CA50_{n+1} = \text{function}(CA90_n, TI, SOI, P_{IVC}, P_{EVO}, P_{NVO}) \quad (2)$$

where n is the cycle iteration index, $CA50$ is the time in $^\circ CA$ where 50% of net heat release has occurred, $CA90$ is the time in $^\circ CA$ when 90% of net heat release has occurred, TI is the injection pulse width in milliseconds, SOI is Start of Injection in $^\circ CA$ Before Top Dead Center ($^\circ BTDC$), and the pressure variables measurements are mean pressures during specific regions of the combustion cycle (see Fig. 3). Details of the simplified net heat release algorithm are available in [4]. Fuel rail pressure is constant; however, the reader should note that the pressure drop to cylinder pressure during NVO injections varies with each transient step and during high CV regions. The cylinder pressure variables P_{IVC} , P_{EVO} , and P_{NVO} were chosen to capture cycle-to-cycle residual coupling and air flow without the difficulties of explicitly modeling those quantities. To meet real-time engine controller timing requirements, P_{IVC} and P_{NVO} have been modified from [4]. P_{IVC} has been moved to the previous cycle, and the range of P_{NVO} 's mean has been shortened. The subscripts IVC, EVO, and NVO refer to the general timing regions Intake Valve Close, Exhaust Valve Open, and Negative Valve Overlap, respectively.

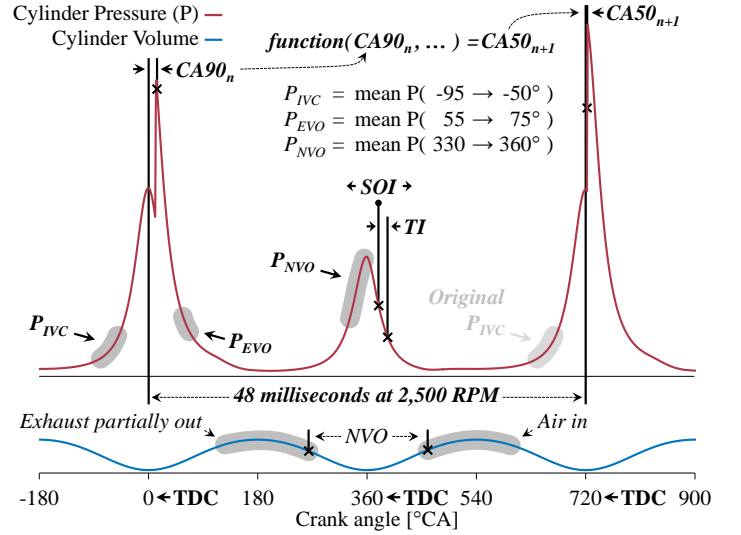


Figure 3: A schematic of key engine cycle variables. The timing of both P_{IVC} and P_{NVO} have been modified from [4] to meet real-time engine controller timing requirements.

WR-ELM Overview

The primary benefits of an ELM approach over the ϵ -SVR method used in [4] are:

- An ELM is easily adapted to online adaptation [17].
- An ELM provides good model generalization when the data are noisy [18].
- An ELM is extremely computationally efficient [17, 18].

WR-ELM is developed in this work as a weighted least squares extension to Online Sequential - ELM [17]. While developed independently, a similar derivation is available in [19]. The difference between this work and the classification application in [19] is the use of a ring buffer data structure “chunk” for online updates to an offline trained regression model.

The data in the WR-ELM ring buffer can be weighted more heavily than the data originally used to fit the offline model. This allows emphasis to be placed on recent measurements that might be between the “quills” of Fig. 2’s offline trained model or the result of day-to-day engine parameter variation. Thus, this approach allows one to prescribe a partitioned balance between the offline model fit against the need to adapt to the most recent conditions. It also explicitly avoids over adaptation to the local conditions (that could compromise global generality) by “forgetting” old ring buffer data that eventually exit the buffer. Fig. 4 gives a schematic representation of this approach.

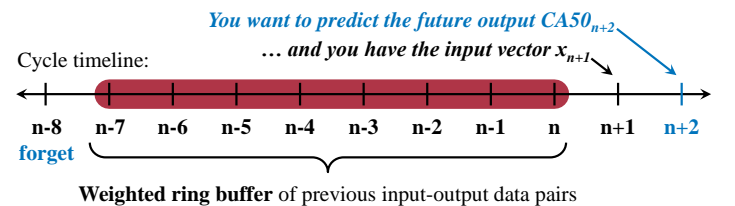


Figure 4: A schematic of overview WR-ELM.

Other differences from [17, 19] are that the derivation below lacks a bias vector b , uses the Gaussian distribution for \mathbf{a} , and drops the unnecessary logistic function exponential negative. It was found empirically that the computation of the bias b addition step could be removed with no loss of fitting performance if \mathbf{a} 's elements were drawn from the Gaussian distribution $\mathcal{N}(0,1)$. ELM theory only requires the distribution to be continuous [18], although the ability to remove the bias is likely problem specific.

WR-ELM Core Algorithm

The basic goal of an Extreme Learning Machine (ELM) is to solve for the output layer weight vector β that scales the transformed input \mathbf{H} to output \mathbf{T} :

$$\mathbf{H}\beta = \mathbf{T} \quad (3)$$

where \mathbf{H} is the hidden layer output matrix of a given input matrix and \mathbf{T} is the target vector. \mathbf{H} can be thought of as a non-linear front-end to the linear β back-end, with β being used to scale the front-end to fit the target vector \mathbf{T} .

For a set of n input-output data pairs and \tilde{N} neurons at the n th cycle timestep, these variables are given by

$$\mathbf{H}(\mathbf{a}, \mathbf{x}) = \begin{bmatrix} G(\mathbf{a}_1, \mathbf{x}_1) & \dots & G(\mathbf{a}_{\tilde{N}}, \mathbf{x}_1) \\ \vdots & \ddots & \vdots \\ G(\mathbf{a}_1, \mathbf{x}_n) & \dots & G(\mathbf{a}_{\tilde{N}}, \mathbf{x}_n) \end{bmatrix}_{n \times \tilde{N}} \quad (4)$$

where $G(\mathbf{a}_i, \mathbf{x})$ is the neuron activation function, chosen to be a commonly used logistic function, but without the unnecessary negative:

$$G(\mathbf{a}_i, \mathbf{x}) = \frac{1}{1 + \exp(\mathbf{x} \cdot \mathbf{a}_i)}. \quad (5)$$

Using a random input weight vector \mathbf{a}_i that is composed of random variable (r.v.) samples from a Gaussian distribution for each of the z input variables gives

$$\mathbf{a}_i = \begin{bmatrix} r.v. \sim \mathcal{N}(0,1) \\ \vdots \\ r.v. \sim \mathcal{N}(0,1) \end{bmatrix}_{z \times 1}. \quad (6)$$

The use of a random \mathbf{a}_i that is re-sampled for each of the \tilde{N} individual neurons during initialization is the main difference of an Extreme Learning Machine vs. conventional neural networks that iteratively train each \mathbf{a}_i [18]. These \mathbf{a}_i vectors can then be collected into a single input weight matrix \mathbf{a} , which is held fixed across all n input row vectors \mathbf{x}

$$\mathbf{x} = [\text{CA90}_n \quad \text{TI} \quad \text{SOI} \quad \text{P}_{\text{IVC}} \quad \text{P}_{\text{EVO}} \quad \text{P}_{\text{NVO}}]_{n \times z} \quad (7)$$

and n output values

$$\mathbf{T} = [\text{CA50}_{n+1}]_{n \times 1}. \quad (8)$$

The normal equations can then be used to solve for the least squares solution $\hat{\beta}$ of Eq. 3 with

$$\hat{\beta} = (\mathbf{H}^\top \mathbf{H})^{-1} \mathbf{H}^\top \mathbf{T}. \quad (9)$$

To extend this to a weighted least squares solution, one can incorporate a diagonal weight matrix \mathbf{W} to the normal equations [20]:

$$\hat{\beta} = (\mathbf{H}^\top \mathbf{W} \mathbf{H})^{-1} \mathbf{H}^\top \mathbf{W} \mathbf{T} \quad (10)$$

The solution can then be split between an offline and a weighted online ‘‘chunk’’ of recent input-output data pairs to avoid computational burden of storing offline data. To do this, the matrices are partitioned with subscript 0 and 1 denoting the offline and online updated components, respectively:

$$\mathbf{H} = \begin{bmatrix} \mathbf{H}_0 \\ \mathbf{H}_1 \end{bmatrix}_{n \times \tilde{N}} \quad \mathbf{W} = \begin{bmatrix} \mathbf{W}_0 & \mathbf{0} \\ \mathbf{0} & \mathbf{W}_1 \end{bmatrix}_{n \times N} \quad \mathbf{T} = \begin{bmatrix} \mathbf{T}_0 \\ \mathbf{T}_1 \end{bmatrix}_{n \times 1} \quad (11)$$

Then, following a similar derivation in [17] for recursive least squares but adding the weight matrix, the inversion portion $\mathbf{H}^\top \mathbf{W} \mathbf{H}$ of the weighted normal equations Eq. 10 can be re-written in terms of \mathbf{K}_0 and \mathbf{K}_1 :

$$\begin{aligned} \mathbf{K}_1 &= \mathbf{H}^\top \mathbf{W} \mathbf{H} = \begin{bmatrix} \mathbf{H}_0 \\ \mathbf{H}_1 \end{bmatrix}^\top \begin{bmatrix} \mathbf{W}_0 & \mathbf{0} \\ \mathbf{0} & \mathbf{W}_1 \end{bmatrix} \begin{bmatrix} \mathbf{H}_0 \\ \mathbf{H}_1 \end{bmatrix} \\ &= \begin{bmatrix} \mathbf{H}_0^\top & \mathbf{H}_1^\top \end{bmatrix} \begin{bmatrix} \mathbf{W}_0 & \mathbf{0} \\ \mathbf{0} & \mathbf{W}_1 \end{bmatrix} \begin{bmatrix} \mathbf{H}_0 \\ \mathbf{H}_1 \end{bmatrix} \\ &= \begin{bmatrix} \mathbf{H}_0^\top \mathbf{W}_0 & \mathbf{H}_1^\top \mathbf{W}_1 \end{bmatrix} \begin{bmatrix} \mathbf{H}_0 \\ \mathbf{H}_1 \end{bmatrix} \\ &= \mathbf{H}_0^\top \mathbf{W}_0 \mathbf{H}_0 + \mathbf{H}_1^\top \mathbf{W}_1 \mathbf{H}_1 \\ &= \mathbf{K}_0 + \mathbf{H}_1^\top \mathbf{W}_1 \mathbf{H}_1 \end{aligned} \quad (12)$$

The non-inverted portion of the normal equations can similarly be re-written using existing relations:

$$\begin{aligned} \mathbf{H}^\top \mathbf{W} \mathbf{T} &= \begin{bmatrix} \mathbf{H}_0 \\ \mathbf{H}_1 \end{bmatrix}^\top \begin{bmatrix} \mathbf{W}_0 & \mathbf{0} \\ \mathbf{0} & \mathbf{W}_1 \end{bmatrix} \begin{bmatrix} \mathbf{T}_0 \\ \mathbf{T}_1 \end{bmatrix} \\ &= \begin{bmatrix} \mathbf{H}_0^\top & \mathbf{H}_1^\top \end{bmatrix} \begin{bmatrix} \mathbf{W}_0 & \mathbf{0} \\ \mathbf{0} & \mathbf{W}_1 \end{bmatrix} \begin{bmatrix} \mathbf{T}_0 \\ \mathbf{T}_1 \end{bmatrix} \\ &= \begin{bmatrix} \mathbf{H}_0^\top \mathbf{W}_0 & \mathbf{H}_1^\top \mathbf{W}_1 \end{bmatrix} \begin{bmatrix} \mathbf{T}_0 \\ \mathbf{T}_1 \end{bmatrix} \\ &= \mathbf{H}_0^\top \mathbf{W}_0 \mathbf{T}_0 + \mathbf{H}_1^\top \mathbf{W}_1 \mathbf{T}_1 \\ &= \mathbf{K}_0 \mathbf{K}_0^{-1} \mathbf{H}_0^\top \mathbf{W}_0 \mathbf{T}_0 + \mathbf{H}_1^\top \mathbf{W}_1 \mathbf{T}_1 \\ &= \mathbf{K}_0 \hat{\beta}_0 + \mathbf{H}_1^\top \mathbf{W}_1 \mathbf{T}_1 \\ &= (\mathbf{K}_1 - \mathbf{H}_1^\top \mathbf{W}_1 \mathbf{H}_1) \hat{\beta}_0 + \mathbf{H}_1^\top \mathbf{W}_1 \mathbf{T}_1 \\ &= \mathbf{K}_1 \hat{\beta}_0 - \mathbf{H}_1^\top \mathbf{W}_1 \mathbf{H}_1 \hat{\beta}_0 + \mathbf{H}_1^\top \mathbf{W}_1 \mathbf{T}_1 \end{aligned} \quad (13)$$

Substituting Eq. 13 into the online solution

$$\begin{aligned} \hat{\beta}_1 &= (\mathbf{K}_1^{-1}) (\mathbf{H}^\top \mathbf{W} \mathbf{T}) \\ &= \hat{\beta}_0 - \mathbf{K}_1^{-1} \mathbf{H}_1^\top \mathbf{W}_1 \mathbf{H}_1 \hat{\beta}_0 + \mathbf{K}_1^{-1} \mathbf{H}_1^\top \mathbf{W}_1 \mathbf{T}_1 \\ &= \hat{\beta}_0 + \mathbf{K}_1^{-1} \mathbf{H}_1^\top \mathbf{W}_1 (\mathbf{T}_1 - \mathbf{H}_1 \hat{\beta}_0) \end{aligned} \quad (14)$$

yields the online solution without the need for the full offline dataset. To trade the computational burden of the $\tilde{N} \times \tilde{N}$ \mathbf{K} inverse for an inverse of the typically smaller sized

ring buffer, one can let $\mathbf{P} = \mathbf{K}^{-1}$

$$\mathbf{P}_0 = \mathbf{K}_0^{-1} = \left(\mathbf{H}_0^\top \mathbf{W}_0 \mathbf{H}_0 \right)^{-1} \quad (15)$$

$$\mathbf{P}_1 = \mathbf{K}_1^{-1} = \left(\mathbf{P}_0^{-1} + \mathbf{H}_1^\top \mathbf{W}_1 \mathbf{H}_1 \right)^{-1} \quad (16)$$

and use the matrix inversion lemma on Eq. 16 to yield:

$$\mathbf{P}_1 = \mathbf{P}_0 - \mathbf{P}_0 \mathbf{H}_1^\top \left(\mathbf{W}_1^{-1} + \mathbf{H}_1 \mathbf{P}_0 \mathbf{H}_1^\top \right)^{-1} \mathbf{H}_1 \mathbf{P}_0 \quad (17)$$

Unlike OS-ELM and WOS-ELM [17, 19], additional simplification is possible because the WR-ELM algorithm does not propagate \mathbf{P}_1 in time. To begin, append the $\mathbf{H}_1^\top \mathbf{W}_1$ portion of Eq. 14 to Eq. 17 and distribute \mathbf{H}_1^\top to give:

$$\begin{aligned} & \mathbf{P}_1 \mathbf{H}_1^\top \mathbf{W}_1 = \\ & \left[\mathbf{P}_0 \mathbf{H}_1^\top - \mathbf{P}_0 \mathbf{H}_1^\top \left(\mathbf{W}_1^{-1} + \mathbf{H}_1 \mathbf{P}_0 \mathbf{H}_1^\top \right)^{-1} \mathbf{H}_1 \mathbf{P}_0 \mathbf{H}_1^\top \right] \mathbf{W}_1 \end{aligned} \quad (18)$$

Eq. 18 can then be simplified with the substitutions $\mathbf{A} = \mathbf{P}_0 \mathbf{H}_1^\top$, $\mathbf{B} = \mathbf{H}_1 \mathbf{A}$ and then distributing \mathbf{W}_1 to provide:

$$\mathbf{P}_1 \mathbf{H}_1^\top \mathbf{W}_1 = \mathbf{A} \left[\mathbf{W}_1 - \left(\mathbf{W}_1^{-1} + \mathbf{B} \right)^{-1} \mathbf{B} \mathbf{W}_1 \right] \quad (19)$$

Transforming Eq. 19 with the identity $(\mathbf{X} + \mathbf{Y})^{-1} \mathbf{Y} = \mathbf{X}^{-1} (\mathbf{X}^{-1} + \mathbf{Y}^{-1})^{-1}$ gives:

$$\mathbf{P}_1 \mathbf{H}_1^\top \mathbf{W}_1 = \mathbf{A} \left[\mathbf{W}_1 - \mathbf{W}_1 \left(\mathbf{W}_1 + \mathbf{B}^{-1} \right)^{-1} \mathbf{W}_1 \right] \quad (20)$$

Eq. 20 is then in a form where the identity $\mathbf{X} - \mathbf{X}(\mathbf{X} + \mathbf{Y})^{-1} \mathbf{X} = (\mathbf{X}^{-1} + \mathbf{Y}^{-1})^{-1}$ can be applied to yield a substantially simpler form with an inverse that is :

$$\mathbf{P}_1 \mathbf{H}_1^\top \mathbf{W}_1 = \mathbf{A} \left(\mathbf{W}_1^{-1} + \mathbf{B} \right)^{-1} \quad (21)$$

Finally, noting that $\mathbf{P}_1 \mathbf{H}_1^\top \mathbf{W}_1 = \mathbf{K}_1^{-1} \mathbf{H}_1^\top \mathbf{W}_1$, one can then substitute Eq. 21 into Eq. 14 and arrive at the following algorithm summary:

OFFLINE TRAINING

$$\mathbf{P}_0 = \left[\left(\mathbf{H}_0^\top \mathbf{W}_0 \mathbf{H}_0 \right)^{-1} \right]_{\tilde{N} \times \tilde{N}} \quad (22)$$

$$\hat{\boldsymbol{\beta}}_0 = \left[\mathbf{P}_0 \mathbf{H}_0^\top \mathbf{W}_0 \mathbf{T}_0 \right]_{\tilde{N} \times 1}$$

ONLINE ADAPTATION

$$\mathbf{A} = \mathbf{P}_0 \mathbf{H}_1^\top, \quad \mathbf{B} = \mathbf{H}_1 \mathbf{A} \quad (23)$$

$$\hat{\boldsymbol{\beta}}_1 = \hat{\boldsymbol{\beta}}_0 + \mathbf{A} \left(\mathbf{W}_1^{-1} + \mathbf{B} \right)^{-1} \left(\mathbf{T}_1 - \mathbf{H}_1 \hat{\boldsymbol{\beta}}_0 \right)$$

ONLINE PREDICTIONS

$$\text{CA50}_{n+2} = \mathbf{T}_{n+1} = \mathbf{H}(\mathbf{a}, \mathbf{x}_{n+1}) \hat{\boldsymbol{\beta}}_1 \quad (24)$$

The reader should note that only \mathbf{P}_0 and $\hat{\boldsymbol{\beta}}_0$ are needed for online adaptation, and the size of these matrices scales only

with an increasing number of neurons \tilde{N} . **None of the original offline data are needed.** Additionally, note that Eq. 24 is simply the reverse of Eq. 3 with the most recent \mathbf{x}_{n+1} cycle vector and $\hat{\boldsymbol{\beta}}_1$ updated from the weighted ring buffer. Finally, it should be mentioned that the resulting update law Eq. 23 is structurally similar that of the Kalman filter [20] which also uses recursive least squares. Future work should look at applying Kalman filtering algorithm improvements (e.g. square root filtering) to WR-ELM.

WR-ELM Usage Procedure

1. Scale \mathbf{x} and \mathbf{T} columns between zero and unity for each variable. For the combustion implementation, column variable values below the 0.1% and above the 99.9% percentile were saturated at the respective percentile value, and then normalized between zero and unity between these percentile based saturation limits. This was done to both adequately represent the distribution tails and avoid scaling issues.
2. The random non-linear front-end transformation that enables the low computational complexity of the WR-ELM algorithm may result in ill-conditioned matrices. All numerical implementations should use double precision. Additionally, one should consider using Singular Value Decomposition for ill-conditioned matrix inversions.
3. Using the $\mathcal{N}(0,1)$ Gaussian distribution, initialize the $z \times \tilde{N}$ ELM input weights \mathbf{a} and hold them fixed for all training / predictions. For the combustion implementation, this was done with MATLAB[®]'s built-in *randn()* function and the Mersenne Twister pseudo random number generator with seed 7,898,198. An \tilde{N} of 64 was used based on initial trials, and each cylinder's individually computed WR-ELM model used an identical input weight matrix \mathbf{a} .
4. Build $\mathbf{H}_0(\mathbf{a}, \mathbf{x}_0)$ from previously acquired samples that cover a wide range of conditions with Eq. 4 using an input matrix \mathbf{x}_0 and output target vector \mathbf{T}_0 (the formats of these are given in Eqs. 7 & 8, respectively). For the combustion implementation, the initial training data were ~40 minutes of random engine set points covering 53,884 cycles and 1,179 random engine set points at a single engine speed, however, it appears that only ~20 minutes of data may be sufficient.
5. Specify a weight matrix \mathbf{W}_0 for offline measurements. For the combustion implementation, a simple scalar value $\mathbf{W}_0 = 2 \times 10^{-3}$ was chosen using a small design of experiments. While this weight works well as a proof of concept, future work should more rigorously determine the weight(s), perhaps with optimization techniques. Note that \mathbf{W}_0 allows weighting to be applied offline and that a small offline weighting is equivalent to a large online weighting.
6. Solve for the offline solution \mathbf{P}_0 and $\hat{\boldsymbol{\beta}}_0$ using Eqs. 22 and hold these values constant for all future predictions.

- At some point far enough into the future to fill the ring buffer, execute the WR-ELM update algorithm between combustion cycle $n + 1$ and $n + 2$ as shown in Fig. 4. Populate the ring buffer of size r with recently completed input-output pairs using:

$$\begin{aligned} \text{input ring buffer} = \mathbf{x}_1 &= \begin{bmatrix} \mathbf{x}_{n-r} \\ \vdots \\ \mathbf{x}_n \end{bmatrix}_{r \times z} \\ \text{output ring buffer} = \mathbf{T}_1 &= \begin{bmatrix} \text{CA50}_{n+1-r} \\ \vdots \\ \text{CA50}_{n+1} \end{bmatrix}_{r \times 1} \end{aligned} \quad (25)$$

For the combustion implementation, r was taken to be 8 cycles after trial and error tuning with existing datasets. If desired, r can vary cycle-to-cycle.

- As with the offline data, build $\mathbf{H}_1(\mathbf{a}, \mathbf{x}_1)$ with Eq. 4 using an input matrix \mathbf{x}_1 and output target vector \mathbf{T}_1 . Specify a weight matrix \mathbf{W}_1 . For the combustion implementation the identity matrix ($\mathbf{W}_1 = \mathbf{I}$) was chosen since weighting was already applied to the offline data in step 5. Gradually increased weighting on the most recent time steps in the ring buffer was explored, however, it did not net a significant improvement to model fitting performance over a simple scalar value on offline data. Although not explored in the current implementation, \mathbf{W}_1 can vary cycle-to-cycle.
- Solve for the updated $\hat{\beta}_1$ solution using Eqs. 23.
- After cycle $n + 1$'s input vector \mathbf{x}_{n+1} is fully populated, transform vector into \mathbf{H}_{n+1} using Eq. 4 and solve for a predicted target value \mathbf{T}_{n+1} or CA50_{n+2} using Eq. 24.
- Repeat steps 7-10 for each new time step.

WR-ELM Real-Time Feasibility Tests

A custom collection of MATLAB[®] software routines was developed using the procedure given in the previous section to run WR-ELM predictions. The offline solution provided by Eqs. 22 was solved at an average rate of 1.1 microseconds per combustion cycle per cylinder on an Intel[®] i7 860 2.8 GHz desktop computer running Gentoo Linux[®]. The online predictions from Eqs. 23, 25, & 24 were recast into a *parfor* loop that automatically parallelized the code across four worker threads to provide predictions at an average rate of 66 microseconds per combustion cycle per cylinder. This level of performance is more than adequate for real-time when a combustion cycle is on the order of ~50 milliseconds. Additionally, execution time was found to be fast enough for real-time on a low-cost Raspberry Pi[®] implementation that is currently in development using the Eigen C++ matrix library.

Experimental Setup

Table 1 provides a summary of the experimental setup and conditions visited. In-cylinder pressure was acquired on a 1.0 °CA basis and pegged thermodynamically for each cycle after IVC using a polytropic exponent of 1.35. This exponent was chosen to most closely match the pegging

Table 1: Experimental setup and test conditions

Engine		
Make / model		GM / LNF Ecotec
Cylinder layout		in-line 4
Overall displacement		2.0 L
Bore / stroke		86 / 86 mm
Geometric compression ratio	(modified from stock engine)	11.2 : 1
Cam lift	(modified from stock engine)	3.5 mm
Cam duration	(modified from stock engine)	93 °CA
Cam phaser type		hydraulic
Fuel injector type		direct, side mounted, wall guided
Fuel		
Designation		Haltermann HF0437, EPA Tier II EEE
Description		U.S. Federal Emission Certification Gasoline
Research Octane Number		97.0
Motor Octane Number		88.1
ASTM D240 heating value		42.8 MJ / kg
Aromatic / olefin / saturate fractions		28 / 1 / 71 % volume
Test conditions		
Throttle position		wide open
Turbocharger		wastegate open
Supercharger		bypassed
Residual retention strategy		negative valve overlap
IVO set point range	(1 st / 99 th percentile)	78.6 / 128 °ATDC
EVC set point range	(1 st / 99 th percentile)	-118 / -83.0 °ATDC
SOI set point range	(1 st / 99 th percentile)	272 / 378 °BTDC
TI set point range	(1 st / 99 th percentile)	0.582 / 1.01 ms
Net IMEP values visited	(1 st / 99 th percentile)	1.85 / 3.62 bar
Air-fuel ratios visited	(1 st / 99 th percentile)	0.90 / 1.6
Estimated fuel per cycle	(1 st / 99 th percentile)	6 / 11 mg
Intake runner temps. across all four cyls.		$\mu = 52.6$ °C, $\sigma = 1.6$ °C
Fuel injection pressure		$\mu = 70.0$ bar, $\sigma = 0.85$ bar
Coolant temperature		$\mu = 89.5$ °C, $\sigma = 3.4$ °C
Engine speed		$\mu = 2,500$ RPM, $\sigma = 6$ RPM

results achieved using the single intake runner high speed pressure sensor on cylinder 1. For the purpose of computing cycle-to-cycle net Indicated Mean Effective Pressure (IMEP), a cycle was defined as starting at 360 °BTDC firing and ending at 359 °ATDC firing. The reference cam lift for timing and duration in Table 1 is 0.5 mm. The air-fuel ratio range indicated in Table 1 was measured post-turbine, and represents a mixture from all four cylinders. Fuel mass per cycle was *estimated* using the fuel's lower heating value, assuming that the gross heat release was 20% greater than the net heat release, and that the combustion efficiency was 100%.

Dataset Description

The full collection of 129,964 cycles is comprised of five ~20 minute random test subsequences. Each random subsequence covers the same nominal ranges listed in Table 1; however, one subsequence holds SOI fixed. The sequence with SOI fixed is only used as part of Fig. 1, and not during the model training and testing presented here. Total cycle counts are reported after outliers are removed. The outlier criteria (detailed in [4]) are fairly permissive and remove only ~3% of the data.

The offline solution was trained using ~40 minutes of test cell time covering 53,884 cycles and 1,179 random engine set points at 2,500 RPM (two random subsequences). The online solution was run with a separate random subsequence and fed unseen cycles one-by-one, similar to what would

be experienced in a real-time implementation. This online dataset is comprised of 25,323 consecutive cycles with 521 random engine set points. Longer online sequences were also tested, and achieved similar results. The 25,323 dataset is the same as the “26,000 dataset” used for training and validation in [4]. The cycle count discrepancy is an unintentional naming mistake due to the partitioning of the full 129,964 dataset into five separate subsets at are nominally 26,000 cycles in length. The reader should note that each random transient step in these datasets is occurring approx. every 0.5 - 10 seconds.

Results & Discussion

The WR-ELM model’s fitting performance on a 25,323 cycle dataset (excluding outliers) is shown in Table 2 and in Figs. 5, 6, and 7. The minimum coefficient of determination (R^2) given in Table 2 shows that at least 79% of the cycle-to-cycle variance can be explained by the model as it is currently defined. This is slightly better than the 76% achieved with ϵ -Support Vector Regression on the same dataset in [4]. However, this is not a 1:1 comparison because WR-ELM is fully predicting the entire 25,323 cycle dataset, whereas ϵ -SVR’s training strategy ensured the data-driven model had partially seen the operating points it was trying to predict. Steady-state RMSE in Table 2 was assessed at a single set point with an all-cylinder mean CA50 of 2.9 °CA After TDC (°ATDC) and mean net Indicated Mean Effective Pressure (IMEP) of 2.8 bar before the transient sequence started.

Table 2: WR-ELM model of Eq. 2 error statistics

Cylinder #	Overall [†] R^2	Overall RMSE [°CA]	Steady-State RMSE [°CA]
1	0.80	1.91	0.90
2	0.80	2.16	0.96
3	0.79	2.25	1.05
4	0.82	1.69	0.86

[†] 25,323 consecutive cycles with random transient steps occurring approx. every 0.5 - 10 sec. and occasional misfires.

Fig. 5 shows the distribution of model errors, and it is clear that there is a slight positive bias to the predictions. Fig. 6 provides insight into the tails of Fig. 5 and shows that model errors still generally capture the correct directionality. Fig. 6 also shows that late phasing is somewhat under predicted, and that the positive bias is largely from the midrange values of CA50. The cycle-to-cycle model fit presented in Fig. 7 shows good agreement, with occasional tracking errors that are quickly corrected by online adaptation. Missing segments are outliers (as defined in the [4] paper) and total only ~3% of the data recorded from experiment. The reader is encouraged to compare and contrast this fit against the partially acausal fit in Fig. 6 of [4] for the same exact experimental subsequence. Fig. 7 also includes colormaps to provide qualitative insight into the model weights and online adaptation behavior. Note that the same non-linear front-end specified by \mathbf{a} is used for each cylinder, and any cylinder-to-cylinder differences in the cycle-to-cycle $\hat{\beta}_1$ are due to different characteristics of each cylinder. The neurons are sorted by the 2-norm of their

respective input weight vector \mathbf{a}_i . Overall, the authors believe the level of fit shown in Table 2 and in Figs. 5, 6, and 7 is very good considering that the dataset includes both transients and operating points with high CV, right up to complete misfire.

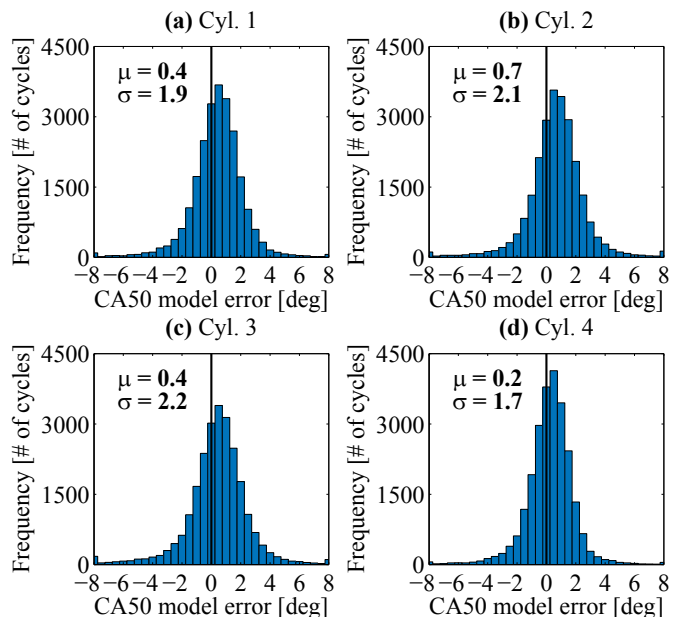


Figure 5: Error histograms for WR-ELM model of Eq. 2 across 25,323 consecutive cycles with random transient steps occurring approx. every 0.5 - 10 sec. and occasional misfires.

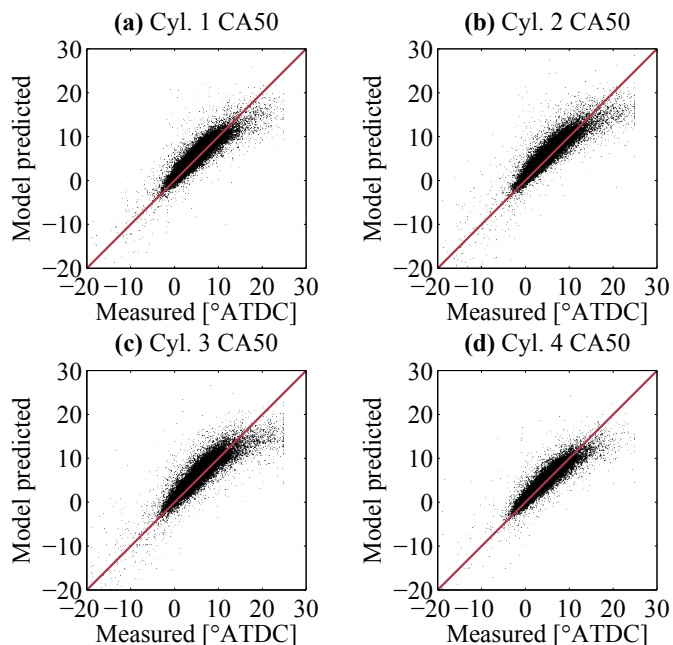


Figure 6: Predicted vs. measured WR-ELM model of Eq. 2 across 25,323 consecutive cycles with random transient steps occurring approximately every 0.5 - 10 sec. and occasional misfires. Late phasing is under predicted, but almost all prediction outliers capture the correct directionality.

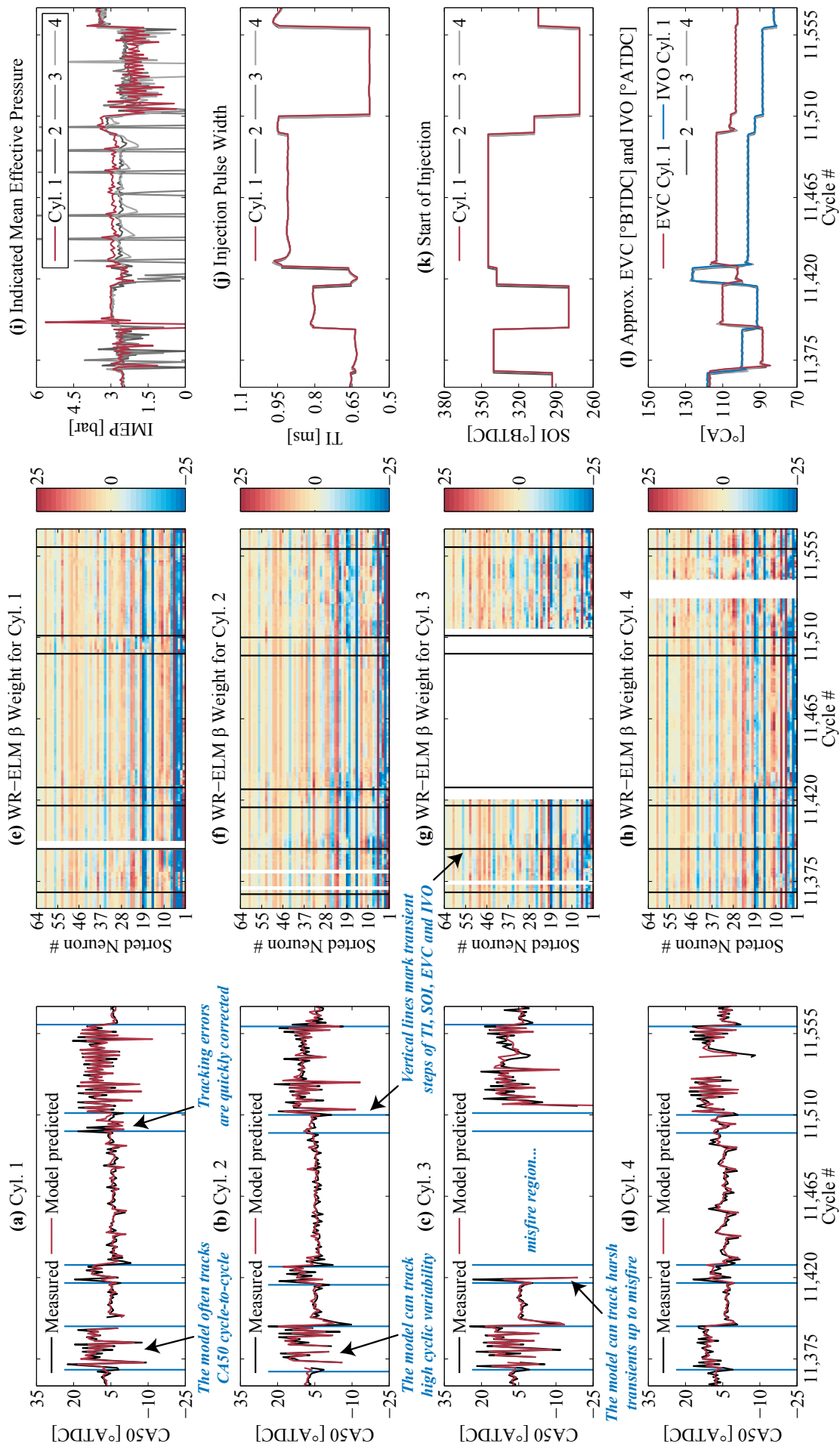


Figure 7: The WR-ELM CA50 model of Eq. 2 can track CA50 through transients every 0.5 - 10 sec., operating points with high CV, and at steady-state during a particularly harsh region of the 25,323 cycle dataset that includes misfires. The colormaps (linearly scaled) provide qualitative insight into the level of cycle-to-cycle adaptation and into cylinder-to-cylinder model differences.

Summary and Conclusion

This work presents a new online adaptation algorithm named Weighted Ring - Extreme Learning Machine. The approach is comprised of a weighted ring buffer data structure of recent measurements that recursively updates an offline trained Extreme Learning Machine solution. The original data do not need to be kept for updates, and only in-cylinder pressure and crank encoder sensors are needed for predictions. While the weight chosen for this model was selected using only a small design of experiments, this fully causal method was shown to provide results as good as or better than the acausal proof of concept ϵ -SVR model presented in [4]. Future work should explore optimal selection of weight(s). The algorithm is fast, and efforts are being made to implement it in real-time on the low-cost Raspberry Pi[®] platform. Finally, the broader objective of this new modeling approach is to enable a new class of cycle-to-cycle predictive control strategies that could potentially bring HCCI's low engine-out NO_x and high fuel efficiency to production feasible gasoline engines.

Acknowledgment

This material is based upon work supported by the Department of Energy [National Energy Technology Laboratory] under Award Number(s) DE-EE0003533. This work is performed as a part of the ACCESS project consortium (Robert Bosch LLC, AVL Inc., Emitec Inc., Stanford University, University of Michigan) under the direction of PI Hakan Yilmaz and Co-PI Oliver Miersch-Wiemers, Robert Bosch LLC.

The authors thank Vijay Janakiraman for providing the raw data analyzed in this paper. The authors also thank Jeff Sterniak for both his test cell and project support. A. Vaughan thanks Nisar Ahmed for many helpful discussions, and his advisor S. Bohac for the freedom to explore the interesting topic of near chaotic HCCI combustion.

References

- [1] L. M. Olesky, J. Vavra, D. Assanis, and A. Babajimopoulos, "Effects of charge preheating methods on the combustion phasing limitations of an HCCI engine with negative valve overlap," *Journal of Engineering for Gas Turbines and Power*, vol. 134, no. 11, p. 112801, 2012.
- [2] A. Babajimopoulos, V. Challa, G. Lavoie, and D. Assanis, "Model-Based Assessment of Two Variable CAM Timing Strategies for HCCI Engines: Recompression vs. Rebreathing," in *Proceedings of the ASME Internal Combustion Engine Division 2009 Spring Technical Conference, ICES2009-76103*, 2009.
- [3] E. A. O. Soto, J. Vavra, and A. Babajimopoulos, "Assessment of residual mass estimation methods for cylinder pressure heat release analysis of HCCI engines with negative valve overlap," *Journal of Engineering for Gas Turbines and Power*, vol. 134, no. 8, p. 082802, 2012.
- [4] A. Vaughan and S. V. Bohac, "A cycle-to-cycle method to predict HCCI combustion phasing," in *Proceedings of the ASME Internal Combustion Engine Division 2013 Fall Technical Conference, ICEF2013-19203*, 2013.
- [5] J. S. Lacey, *The effects of advanced fuels and additives on homogeneous charge compression ignition combustion and deposit formation*. PhD thesis, University of Michigan, 2012.
- [6] A. Vaughan and G. Delagrammatikas, "A high performance, continuously variable engine intake manifold," SAE Paper 2011-01-0420, 2011.
- [7] C. S. Daw, R. M. Wagner, K. D. Edwards, and J. B. G. Jr., "Understanding the transition between conventional spark-ignited combustion and HCCI in a gasoline engine," *Proceedings of the Combustion Institute*, vol. 31, no. 2, pp. 2887 – 2894, 2007.
- [8] E. Hellström, A. G. Stefanopoulou, and L. Jiang, "Cyclic variability and dynamical instabilities in autoignition engines with high residuals," *IEEE Transactions on Control Systems Technology*, vol. 21, no. 5, pp. 1527–1536, 2013.
- [9] J. C. Kantor, "A dynamical instability of spark ignited engines," *Science*, vol. 224, no. 4654, pp. 1233–1235, 1984.
- [10] L. Manofsky, J. Vavra, D. Assanis, and A. Babajimopoulos, "Bridging the gap between HCCI and SI: Spark-assisted compression ignition," SAE Paper 2011-01-1179, 2011.
- [11] M. Sjöberg, J. E. Dec, A. Babajimopoulos, and D. Assanis, "Comparing enhanced natural thermal stratification against retarded combustion phasing for smoothing of HCCI heat-release rates," SAE Paper 2004-01-2994, 2004.
- [12] M. Mehl, W. J. Pitz, M. Sjöberg, and J. E. Dec, "Detailed kinetic modeling of low-temperature heat release for prf fuels in an hcci engine," SAE Paper 2009-01-1806, 2009.
- [13] G. Kukkadapu, K. Kumar, C.-J. Sung, M. Mehl, and W. J. Pitz, "Experimental and surrogate modeling study of gasoline ignition in a rapid compression machine," *Combustion and Flame*, vol. 159, no. 10, pp. 3066 – 3078, 2012.
- [14] G. M. Shaver, *Physics-Based Modeling and Control of Residual-Affected HCCI Engines using Variable Valve Actuation*. PhD thesis, Stanford University, 2005.
- [15] J. Livengood and P. Wu, "Correlation of autoignition phenomena in internal combustion engines and rapid compression machines," *Symposium International on Combustion*, vol. 5, no. 1, pp. 347–356, 1955.
- [16] V. Cherkassky and F. Mulier, *Learning from Data: Concepts, Theory, and Methods*. Wiley, 2007.
- [17] N.-Y. Liang, G.-B. Huang, P. Saratchandran, and N. Sundararajan, "A fast and accurate online sequential learning algorithm for feedforward networks," *Neural Networks, IEEE Transactions on*, vol. 17, no. 6, pp. 1411–1423, 2006.
- [18] G.-B. Huang, Q.-Y. Zhu, and C.-K. Siew, "Extreme learning machine: Theory and applications," *Neurocomputing*, vol. 70, no. 1-3, pp. 489 – 501, 2006.
- [19] B. Mirza, Z. Lin, and K.-A. Toh, "Weighted online sequential extreme learning machine for class imbalance learning," *Neural Processing Letters*, pp. 1–22, 2013.
- [20] D. Simon, *Optimal State Estimation: Kalman, H Infinity, and Nonlinear Approaches*. Wiley-Interscience, 2006.

DISCLAIMER: This report was prepared as an account of work sponsored by an agency of the United States Government. Neither the United States Government nor any agency thereof, nor any of their employees, makes any warranty, express or implied, or assumes any legal liability or responsibility for the accuracy, completeness, or usefulness of any information, apparatus, product, or process disclosed, or represents that its use would not infringe privately owned rights. Reference herein to any specific commercial product, process, or service by trade name, trademark, manufacturer, or otherwise does not necessarily constitute or imply its endorsement, recommendation, or favoring by the United States Government or any agency thereof. The views and opinions of authors expressed herein do not necessarily state or reflect those of the United States Government or any agency thereof.